ACS APPLIED MATERIALS & INTERFACES

Research Article

Cite This: ACS Appl. Mater. Interfaces 2019, 11, 19679−19690

www.acsami.org

Fabrication of Designable and Suspended Microfibers via Low-Voltage 3D Micropatterning

Elisabeth L. Gill,[†,‡] Samuel Willis,[†] Magda Gerigk,[†,‡] Paul Cohen,[†] Duo Zhang,[†,‡] Xia Li,[†] and Yan Yan Shery Huang*[,†,‡]

[†]Department of Engineering, University of Cambridge, Trumpington Street, Cambridge CB2 1PZ, U.K.

[‡]The Nanoscience Centre, University of Cambridge, 11 JJ Thomson Avenue, Cambridge CB3 0FF, U.K.

Supporting Information

ABSTRACT: Building two-dimensional (2D) and three-dimensional (3D) fibrous structures in the micro- and nanoscale will offer exciting prospects for numerous applications spanning from sensors to energy storage and tissue engineering scaffolds. Electrospinning is a well-suited technique for drawing micro- to nanoscale fibers, but current methods of building electrospun fibers in 3D are restrictive in terms of printed height, design of macroscopic fiber networks, and choice of polymer. Here, we combine low-voltage electrospinning and additive manufacturing as a method to pattern layers of suspended mesofibers. Layers of fibers are suspended between 3D-printed supports in situ in multiple fiber layers and designable orientations. We examine the key working parameters to attain a threshold for fiber suspension, use those behavioral observations to establish a "fiber suspension indicator", and demonstrate its utility through design of intricate suspended fiber architectures. Individual fibers produced by this method approach the micrometer/submicrometer scale, while the overall suspended 3D fiber architecture can span over a centimeter in height. We demonstrate an application of suspended fiber architectures in 3D cell culture, utilizing patterned fiber topography to guide the assembly of suspended high-cellular-density structures. The solution-based fiber suspension patterning process we report offers a unique competence in patterning soft polymers, including extracellular matrix-like materials, in a high resolution and aspect ratio. The platform could thus offer new design and manufacturing capabilities of devices and functional products by incorporating functional fibrous elements.

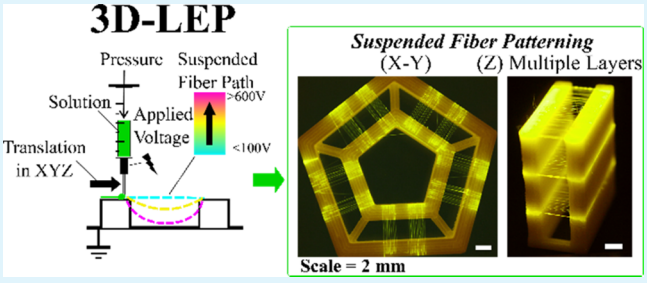

KEYWORDS: *additive manufacturing, 3D printing, mesostructures, fiber patterning, solution processing, electrospinning, 3D cell culture*

1. INTRODUCTION

Micro- and nanostructured fibers have found promising applications in a number of emerging fields including catalysis, energy storage, biosensors, drug delivery, and tissue engineering scaffolds.[1−6] There is potential to realize further advanced material functionality and performance through innovation of high-resolution patterning processes for a broad palette of materials, specifically, in terms of designed individual fiber placement and morphology in addition to the collective fibrous architecture.[7−10]

Electrospinning is a well-established and simple method to draw nano- to microscale fibers by applying a high voltage to a polymer solution or melt, typically yielding mats of randomly positioned mesofibers on the top of a substrate.[10−12] Advances in precision electrospinning methodologies, such as near-field electrospinning, electrohydrodynamic writing, and direct writing electrospinning,[13−21] have led to a significant progress in controlling fiber placement on a substrate compared to conventional "far-field" electrospinning configurations. Several strategies have sought to reduce the high electric field, which is characteristic of electrospinning, through the use of the pyroelectric effect[20,21] or mechanical initiation of a fiber through contact with a sharp edge or point.[22−24] In addition to improving patterning control, the comparatively mild processing conditions permit patterning of electrically sensitive[25] or delicate biological materials.[24]

Extending the patterning capability of electrospun fibers to three dimensions is also a highly desirable innovation target. Thicker fibrous structures can be formed by folding or layering electrospun mats with manual intervention.[26,27] Suspended layered membranes can be formed using separated guiding electrodes,[28,29] and orderly stacked fibers have been demonstrated using melt electrospinning[18,30] or directed electrohydrodynamic printing.[13−15,31] Integrating electrospinning with other printing mechanisms, for example, with polymer extrusion[32,33] or hydrogel printing,[34−36] has also been

Received: January 20, 2019
Accepted: May 13, 2019
Published: May 13, 2019

DOI: 10.1021/acsami.9b01258
ACS Appl. Mater. Interfaces 2019, 11, 19679−19690

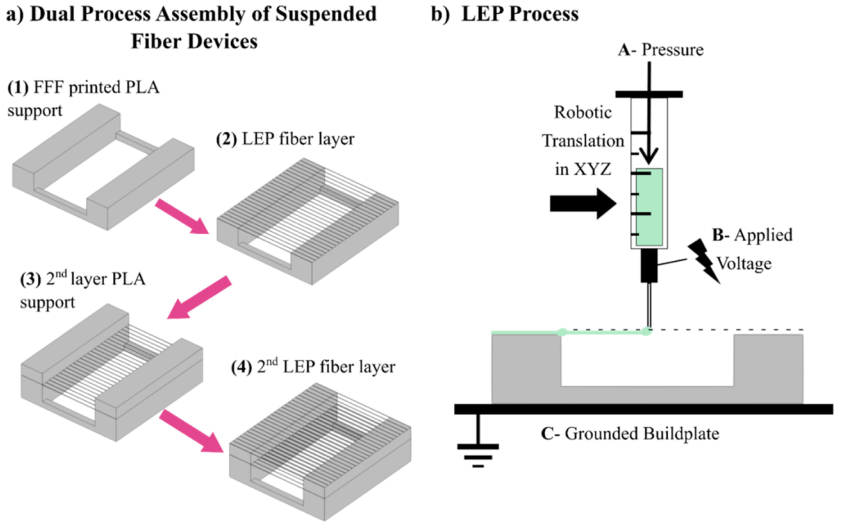

Figure 1. System overview. (a) Depiction of a structure produced layer-by-layer by alternating between the FFF and LEP processes. (b) Experimental configuration.

reported. Building on this progress, there are still several remaining challenges that would be worthwhile addressing.

The above work that patterns fibers with precision in three dimensions is confined to thermoplastic polymers or has limited substrate versatility due to mechanistic restrictions. The approach of direct fiber stacking has a finite patterning height as the residual charge accumulates within the fibers,[30,37] unless local electric grounding is employed.[13] One strategy to pattern fibers within a larger 3D volume is to design free-spanning fiber architectures;[27−29] however, this depends on some form of tethering to a substrate, which can hinder design versatility. In this context, tremendous opportunity exists in designing new strategies to build nano- and microscaled fiber structures in 3D that exhibit novel design capabilities with a broad palette of materials. In particular, methodologies that can enable mesofiber patterning with spanning architectures in three-dimensional space, built into freestanding devices, and allow for versatile fiber chemistry could create new areas of applications.

Building on our existing 2D work, in this manuscript we significantly extend the patterning capabilities of low-voltage electrospinning (LEP)[23] to 3D through integration with fused filament fabrication (FFF) 3D printing. In the following, we will term this integrated printing process to be "3D-LEP". To our knowledge, this is the first systematic exploration of patterning suspended solution electrospun fibers utilizing 3D printing as an in situ tethering mechanism. This strategy can design the suspended fiber architecture, producing versatile freestanding fibrous devices exceeding a centimeter in height.

By utilizing solution-based electrospinning, the method is, in principle, capable of producing functional fibers from a vast library of materials. This has the potential to include over 100 types of natural and synthetic polymers,[1−5] composite fibers, and inorganic/ceramic fibers[28] facilitated by sol−gel chemistry. Furthermore, living systems such as bacteria[23] and mammalian cells[38−40] have been processed into fibers by variations of solution-based electrospinning.

LEP permits polymeric jet initiation at low voltages by interrupting the droplet surface tension by pulling it across "initiating" structures, which sandwich the desired fiber patterning area and aid in mechanical fiber thinning. In 3D-LEP, we combine two existing processes, LEP and FFF, so that the initiating structures are printed in situ. This extends their functionality from merely being a support pillar to facilitating layering of suspended fibers and templating of their suspended behavior, attaining suspended structures that neither LEP nor FFF could achieve independently. Hereafter, we refer to them as "support structures" in this work. While we have utilized FFF printing to form the fiber support structure, other extrusion-based techniques would be equally applicable.[33,34] To summarize our observations of 3D fiber suspension patterning, we present a "parametric space" correlating the fiber 3D configurations to key operation parameters, elucidating the capabilities and limits of our current experimental set-up. We demonstrate hybrid material structures of electrospun mesofibers of gelatin (a polypeptide with many applications in biosensing, drug delivery, and tissue engineering[41−43]) interfaced with a polylactic acid (PLA, a commonly used material in fused filament fabrication (FFF) printing) support structure. By developing the system on a commercially available open-source 3D printer, it was possible to carry out the necessary customization by modifying other open-source projects. The tool-heads were designed to achieve robust tool-head positioning when switching between the LEP and FFF mechanisms based on precision engineering kinematic principles.[44] Mechanical characterization of the patterned fibers was performed to determine their quality and reproducibility. Beyond the scope of this initial study, we foresee that this mesofiber patterning methodology can be adapted to diverse functional material combinations, accessing a unique combination of ink viscoelasticity and feature size, which was previously inaccessible in 3D.

2. RESULTS AND DISCUSSION

Figure 1 illustrates the methodology of 3D-LEP. The FFF process prints a support structure, which has the dual function of fiber initiation via LEP, as well as acting as a support structure for fiber suspension in multiple layers. Computer-aided design and positioning of the FFF printed non-fibrous structure provide control over the suspended fiber structures both in-plane and in height. In a typical print shown in Figure 1a, the FFF tool-head first prints the prescribed PLA support

DOI: 10.1021/acsami.9b01258
ACS Appl. Mater. Interfaces 2019, 11, 19679−19690

structure; the tool-head is then exchanged for an LEP tool-head for fiber deposition. A pneumatic pump (symbolized by A in Figure 1b) drives the flow rate of the polymer solution in a syringe within the LEP tool-head so that an electrospinning droplet forms on the syringe tip. A voltage source (symbolized by B in Figure 1b) applies an electric field between the droplet and grounded build plate (C in Figure 1b). This tensile force stretches the droplet. Contact of the droplet with the surface of a PLA support initiates fiber formation, drawing a fiber to bridge the gap formed by the PLA support structure. After fiber patterning is completed in one layer, the stage is moved downward by a small distance, and the tool-head carrier exchanges tool-heads to return to the FFF process, building a new layer of support structure and thus repeating the layering process.

To achieve the interchange between printing processes within a given print, two critical design considerations were identified for the tool-head "pick-up" and "drop-off" mechanisms. First, the mechanism should achieve this without introducing tool offsets from either misalignment during the tool-changing mechanism itself or any necessary manual handling in between prints such as installation of electrospinning solution. Second, maintaining the correct height between the syringe tip and substrate is crucial to produce fibers reproducibly during electrospinning patterning. Carefully designed tool exchange between the printing processes within a print ensures planar alignment between layers of different materials placed by their respective tools.

Three benchmark goals were set to ensure that the 3D-LEP configuration could fulfill its intended performance. The first of these is that the diameter of the electrospun fibers should be less than 5 μm, motivated by the size of fibers required for applications such as tissue engineering scaffolds.[45] Second, the precision of fiber placement in the *XY* plane should be less than 50 μm. Finally, the *Z* position precision of the electrospinning syringe must be less than 50 μm due to the sensitivity of both the electrospun fiber diameter and initiation of electrospinning to the height of the needle above the collector. Section I of the Supporting Information provides detailed descriptions of the tool-head design. Figure S1 illustrates how kinematic coupling[44] and other engineering design principles can lead to adequate printer performance on a readily available FFF printer. Figure S2 shows how image analysis assessed the tool-head positioning precision in *XYZ* after exchanging tool-heads.

2.1. Working Parameters. Similar to conventional electrospinning, LEP relies on a number of working parameters to control the fiber deposition. These parameters include the intrinsic polymer solution properties; external operating conditions such as the applied voltage, nozzle to substrate distance, and solution flow rate; and environmental factors such as temperature and humidity.[46] Here, a gelatin solution with a composition previously demonstrated for LEP[23] is selected as the model system. If one were to consider switching the polymer solution, key considerations would relate to the responsiveness of the solution to mechanical drawing and sensitivity to an applied electric field. In particular, experimental conditions such as the applied voltage, flow rate, local temperature, and separation distance between the support structures would need to be adapted to suit the polymer concentration, molecular weight, solvent volatility,[22] and overall solution conductivity.[25]

For integrating LEP in 3D, the nozzle-to-ground plate distance increases continuously as a 3D construct is built up layer by layer. Instead of keeping the distance between the syringe tip and grounding plate constant, the distance between the electrospinning syringe needle and the top surface of the PLA support structure was kept constant to maintain the force applied for fiber initiation. The tool-head translation assists fiber thinning, which is set at a constant speed of 100 mm/s. The intention was to work with a constant flow rate of 0.1 μL/min as previous experience in 2D indicated that it was optimal for processing that specific solution. The pneumatic pump produced some variation at a flow rate of that low magnitude due to the compressible nature of air. In this configuration, the applied voltage may be utilized as a direct control parameter to adjust the suspended fiber morphology and assembly. The geometry of the PLA support structure interplays with how voltage influences fiber suspension in 3D. Parameters investigated include the support structure height (*H*), pillar separation length (*L*), and interfiber distance (*P*), as indicated in Figure 2a. For example, fibers spun over a PLA support

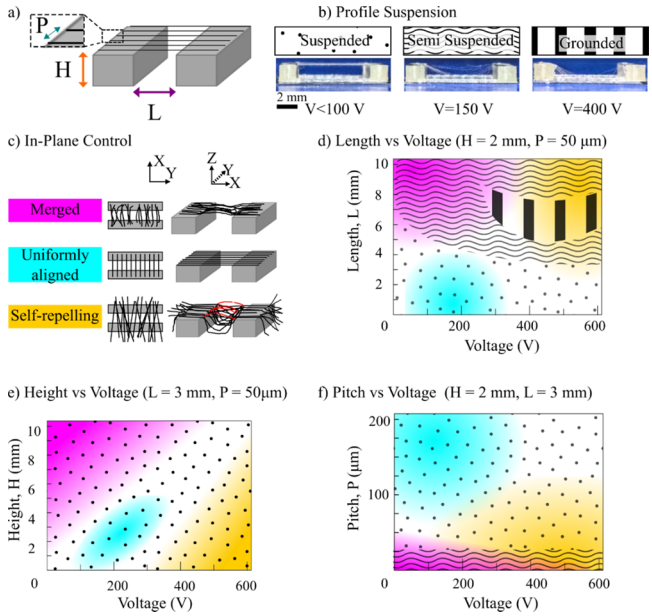

Figure 2. Parametric characterization for fiber suspension. (a) The FFF-printed support structures have a standardized set of geometric parameters of length (*L*), height (*H*), and pitch (*P*) between fibers. (b) Assessment criteria for profile fiber suspension with typical photographs and diagram key. (c) Assessment criteria for in-plane fiber patterning with color coding and illustrative diagrams; uncolored regions of the phase diagrams represent transition regions of in-plane behavior. (d) Phase diagram characterizing fiber suspension behavior for scaffold heights versus voltages. (e) Phase diagram characterizing fiber suspension behavior for initiator separation lengths versus voltages. (f) Phase diagram characterizing fiber suspension behavior for interfiber pitches versus voltages.

structure with H = 2 mm and L = 5 mm, with an applied voltage of below 100 V, leads to a suspended fiber layer (Figure 2b). As the applied voltage is increased, the fibers become attracted to the grounded build platform, transitioning from being suspended to being partially suspended to become completely attracted to the grounded plate. To design future suspended fiber structures, a predictive parametric guide was

DOI: 10.1021/acsami.9b01258
ACS Appl. Mater. Interfaces 2019, 11, 19679−19690

devised to avoid an inefficient trial-and-error process (see further analysis below).

2.2. Parametric Study for Suspended Fiber Patterning. Pilot experiments identified the need to study the interplay between PLA support structure geometric parameters and applied voltage, finding significant effects to suspended fiber layer morphology. The geometric parameters that have the most obvious effect on fiber suspension are L, H, and P, with respect to voltage. Fiber layers were assessed for their global morphology in terms of two sets of criteria: profile suspension and in-plane pattern. Profile suspension is as discussed above and is illustrated by Figure 2b. In-plane patterning refers to how the fiber placement follows its prescribed design: morphology is categorized as merged, uniformly aligned, or self-repelled (see Figure 2c). The presence of excessive residual charge can lead to fibers repelling each other, resulting in a mixture of suspended, grounded, and arched fibers between the support structure pillars and static fibers at the edges, as indicated in red in Figure 2c. Thus, within specific regions of voltage and support structure geometry, it is possible to attain uniformly aligned fibers in suspension. To summarize the experimental observations, Figure 2d shows how fiber morphology is modulated by the interplay between separation length and voltage. Figure 2e maps the height and voltage, and Figure 2f maps the pitch and voltage. Figure S3 provides a selection of raw data that informed these schemes. The subsequent section discusses the theory to interpret these findings.

2.3. Analysis of Fiber Suspension Behavior. To analyze fiber suspension in a given plane, consider the forces acting downward on a fiber (F_t) as it initiates across a support structure pillar, as depicted in Figure 3a,b. The two most

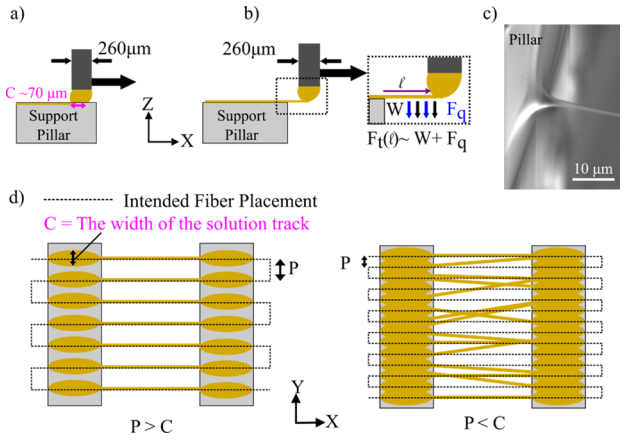

Figure 3. Analysis of fiber initiation and merging. (a) Illustration of a droplet of solution drawing across an initiator and then (b) initiating a fiber over the edge with the forces annotated on the fiber. (c) Scanning electron microscopy image of fiber initiation. (d) Schemes showing scenarios of discrete and overlapping solution tracks, with the influence this has over patterning accuracy.

significant force components acting downward are the fiber weight (W) and electrical attraction (F_q) to the grounded build plate. For the first component, it can be assumed that the fiber weight is proportional to the length l of the fiber drawn, that is, $W \approx k_1 l$. For the attractive force due to electrical charge, F_q, one may assume that the amount of immediate charge accumulation on the fiber is proportional to the length of fiber drawn, F_q, with the form of $F_q \approx qE \approx k_2 lV/H$. Here, q is the charge, E is the electric field, V is the voltage, and H is the initiator height. Combining the two above force components, the forces acting downward on a fiber (F_t) are expressed in eq 1.

$$F_t \approx k_1 l + k_2 \cdot \frac{Vl}{H} \tag{1}$$

Here, k_1 and k_2 are constants. As the length over which the fibers are suspended increases, the forces acting downward on a fiber increase regardless of the applied voltage. Once the applied voltage increases beyond a certain threshold, fibers start falling out of suspension due to the electric field, even over lengths where fibers could otherwise fully suspend. When the applied voltage is below the threshold, the drawing effect on the fiber is purely driven by material viscosity and mechanical elongation. The ability of a solution to sustain fiber initiation from a viscous droplet depends on the nature of polymer entanglement, which relates to polymer molecular weight, concentration, solvent conditions, and other parameters that affect viscosity.[22] Regardless of those factors, fiber initiation becomes difficult to sustain over longer distances without regular interruption of the droplet as the surface tension can overcome the comparatively low electric field in contrast to other electric-jet writing technologies. This can cause capillary breakup on the drawn fiber,[22] leaving an untethered fiber drawn to the grounded build plate.

As H, the height of the support structure from which the fibers are suspended from increases, the intensity of the applied electric field decreases. In this scenario, mechanical elongation becomes the lead driving force for fiber initiation as the electric field strength is comparatively weak. At low applied voltages, solution surface tension overpowers tensile fiber initiation. This causes capillary breakup, leading to fiber withdrawal back into the droplet deposited at the edge of the support structure or merging with neighboring fibers. Increasing the applied voltage to the droplet helps re-adjust the electric field and aids in the initial ejection of a fiber from a viscous droplet, but it also increases fiber self-repulsion. This effect at its extreme can cause fibers to arch over the suspended region, disrupting the ordered placement of fibers.

Next, the in-plane fiber merging behavior and the effect of interfiber pitch are considered. Fiber layers with an interfiber spacing at 50 μm or below can suffer from visible fiber merging in-plane as Figure 2f indicates. The syringe tip used throughout the experiments corresponds to an inner diameter of ~260 μm. When the syringe needle moves across the support structure, it leaves a track of solution before initiating a fiber over the edge by the solution droplet meniscus (Figure 3c). The width of a track of solution left across a support structure, C, correlates to the diameter of the syringe needle and the solution flow rate. At an interfiber spacing of <100 μm, there is a high probability that the solution tracks will overlap, leading to a nonsingular meniscus for fiber initiation, as illustrated in Figure 3d. Upon inspection of well-separated fibers and merged fibers, the solution tracks preceding the merged fibers were mostly indistinguishable. In contrast, for an interfiber pitch of 100–200 μm, the preceding solution tracks for each fiber were clearly separated, as shown in Figure 4a. This produced a regular in-plane fiber pattern on the support structure, following the designed fiber pattern.

To summarize the above discussion, one can assume that, by exceeding some critical force threshold, f^*, the drawn fibers bend toward the ground. Thus, if $F_t/f^* > 1$, grounded or

DOI: 10.1021/acsami.9b01258
ACS Appl. Mater. Interfaces 2019, 11, 19679–19690

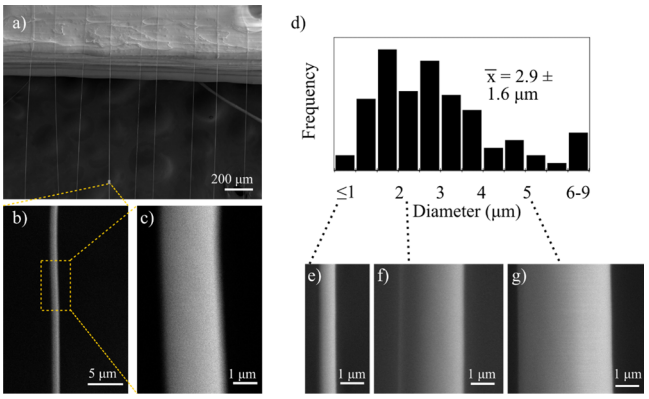

Figure 4. Microstructure characterization within a suspended layer of fibers. An SEM image of a layer of suspended fibers shown in (a) a single fiber is presented at different magnifications in (b) and (c). (d) Histogram of the measured individual fiber diameters with (e)−(g) showing SEM images of fibers at the lower, median, and upper size range, respectively.

loosely hung fibers will be drawn; otherwise, the fibers will remain suspended. Based on transition conditions identified in Figure S3a,b (V = 400 V, H = 3 mm, and L = 3 mm; V = 150 V, H = 2 mm, and L = 5 mm), values for k_1 and k_2 can be determined for eq 1. Based on this, eq 2 presents an approximated fiber "suspension indicator" I_s

$$I_s = L\left(27.5 + 0.0023 \cdot \frac{V}{H}\right) \tag{2}$$

Calculating I_s for different applied voltages and support structure conditions provides a prediction for fiber suspension behavior by comparing the value of I_s to unity, that is, $I_s > 1$ for grounded and $I_s \leq 1$ for suspension. Although the proposed analysis is highly approximated, calculating the I_s values for the experimental conditions of the suspended fiber sample morphologies shown in Figure S3 yields good agreement. Similar analysis could be applied to other solution systems, interfiber spacings, and drawing speeds, accordingly changing the corresponding k_1 and k_2 values.

2.4. Characterization of Mesofiber Microstructure and Mechanical Properties. Figure 4a depicts a sample with both complete fiber suspension and relatively uniform in-plane arrangement. Scanning electron microscopy (SEM) was employed to examine the suspended microstructure and characterize a typical fiber diameter under these conditions, as displayed in Figure 4a−g. Figure 4b,c shows two magnifications of a single fiber, showing a uniform diameter and smooth surface. The histogram in Figure 4d measures the variation in individual fiber diameter, with a mean of 2.9 ± 1.6 μm. Figure 4e−g displays individual fibers at the lower, median, and upper size range of the measured fibers, presented at the same magnification for comparison. Although a spread of fiber diameters exists in the current setup, such diameter deviation is comparable to other solution-based far-field electrospinning processes.[47] An earlier study, presented in Figure S4, identified significantly greater size variation evident due to fiber merging.

A three-point extension test was performed to characterize the tensile mechanical property of the suspended fibers, following previously established methods.[48,49] The applied force per unit fiber (F) was measured as a function of the deflection (δ) in the center of the suspended fiber region (see Figure S5). The extension tests were conducted on samples with PLA support pillar separation distances of L = 2, 3, and 5 mm, with three to six repeats for each separation distance. Figure 5 summarizes the associated $F-\delta$ curves. Fitting the $F-\delta$ curves with eq 3[48−50] (valid for small deflections) thus gives an estimated mean fiber Young's modulus of $E_y \approx 20$ MPa and a mean residual tension of $T_0 \approx 0.05$ mN.

$$F = 4T_o\frac{\delta}{L} + 8AE_y\left(\frac{\delta}{L}\right)^3 \tag{3}$$

The fitted Young's modulus sits at the lower limit compared to the values reported in the literature for far-field electrospun gelatin fibers (i.e., in the range of 25−170 MPa depending on the solution conditions and fiber alignment[51−53]). Enhanced mechanical properties have been demonstrated previously by systematically creating interconnecting fiber junctions,[54] and the effect of fiber alignment and planar patterning has been shown to improve the toughness of nanofiber-reinforced hydrogel composites.[55] It is of note that, beyond the small deflection regions, fibers start to yield or fracture at different deflection levels, leading to varied behavior across different samples. Overall, results from the three-point extension test imply that the gelatin mesofibers produced by the 3D-LEP

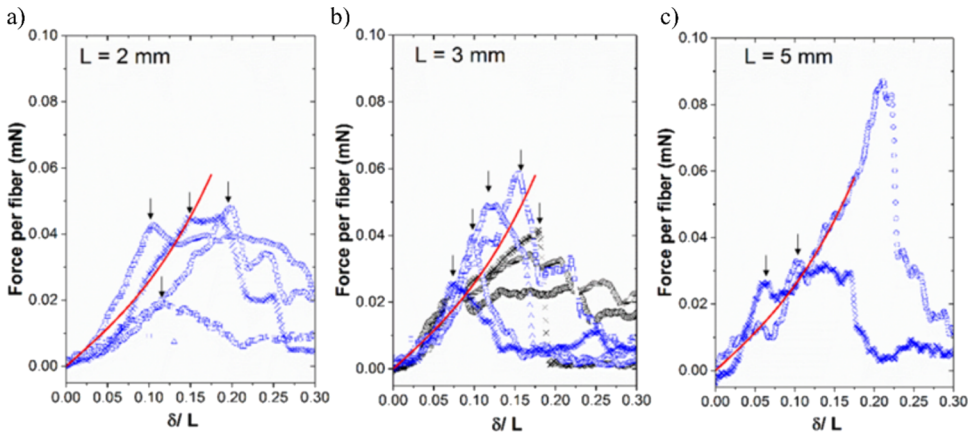

Figure 5. Mechanical assessment of Young's modulus for a suspended fiber layer. The mean applied force per fiber is measured against the ratio of fiber deflection over the scaffold separation length for three frame separation lengths of (a) 2 mm, (b) 3 mm, and (c) 5 mm. The continuous line indicates a fitted solution based on a three-point extension test using a fiber Young's modulus of 20 MPa and residual tension of 0.05 mN.

DOI: 10.1021/acsami.9b01258
ACS Appl. Mater. Interfaces 2019, 11, 19679−19690

technique lead to relatively repeatable elastic fiber properties but can impart different defect levels in the fibers in different printing runs. Thus, it is envisaged that the current 3D-LEP structures are sufficient for applications within the elastic limit of the fibers. Further improvement in processing and solution conditions could be used to adjust fiber fracture properties as required; for example, other focused electrospinning studies have explored.[54]

2.5. Suspended Mesofibrous Architectures in 3D. Mesofiber architectures were designed as individual objects in CAD, assembled in slicing software, and translated into G-code commands for the 3D-LEP platform. To verify the performance of the 3D-LEP system empirically, fiber layers in multiple orientations and varied numbers of layers and spacing were fabricated, as illustrated in Figure 6 and Figure S6. Fluorescein

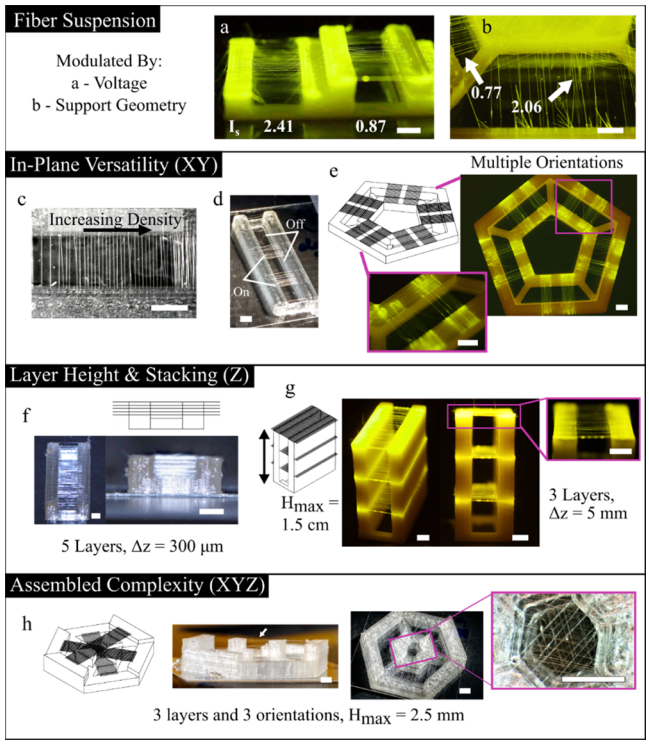

Figure 6. Design of 3D mesofiber architectures. The extent to which fibers are patterned in suspension can be modulated by (a) voltage and (b) support structure geometry. The numbers in white correspond to the suspension parameters for each scenario. Planar patterns include (c) changes in fiber density and (d) discrete patterning of fiber sections. (e) Multiple fiber orientations as designed in CAD. (f) Closely packed fiber layers. (g) Fiber layers up to 1.5 cm in height. (h) Combining multiple fiber layers and orientations gives patterning complexity in 3D. All scale bars, 2 mm.

dye was added to the electrospinning solution to aid in the visualization of fibers at the macroscale in Figure 6a,b,e,g. Control of fiber suspension is shown utilizing voltage and support structure geometry in Figure 6a,b, respectively. The annotated I_s values in white show that these example constructs follow the threshold conditions for suspension outlined above and that the proposed model can be used to guide suspension patterns. Figure S6 illustrates further examples of suspended fiber architectures with their accompanying I_s numbers. This provides further validation that the fiber suspension indicator I_s can extend to predicting fiber suspension in multiple layers reliably for a specific electrospinning solution. Performing this simple calibration for a given solution could significantly reduce the optimization process required for future designs.

The possibility for versatile planar patterning is shown in Figure 6c–e, which is made possible with the robotic control of the 3D printer in *XY* axes. To demonstrate multilayer control, the close packing density in Figure 6f illustrates five visually aligned, suspended fiber layers separated by a height of ∼300 μm at the transition where each layer is visually distinguishable. Figure 6g shows a three-layer structure with fiber layers patterned at 0.5, 1, and 1.5 cm above the printing build platform. Operating within a suspension indicator of less than 1, all the three fiber layers remain in suspension with ordered patterns. Finally, combining planar patterning and layer patterning provides novel assembled complexity; Figure 6h provides an example of fibers patterned on the faces of a hexagon at three different heights. The above examples of 3D suspended fiber patterning would be impossible to produce without an additive layer-manufacturing approach to assemble suspended fiber devices.

In contrast to many traditional microfabrication approaches, the patterning speed of the microscale features is relatively rapid at 100–150 mm/s, while the equipment is straightforward and adaptable. The majority of the time to create suspended fiber structures is consumed by printing the support structure, not the fibers themselves. For example, printing the discrete pattern in Figure 6d takes around 6 min, whereas the tall structure in Figure 6g takes 45 min. Overall, the 3D-LEP configuration provides a rapid mesofiber patterning approach, with enhanced patterning flexibility and the potential to customize with different building materials for both the support structure and mesofibers.

2.6. Applications in Suspended 3D Cell Culture. It is widely accepted by the biomedical research community that, in many cases, cells grown in 3D behave in a more representative manner to in vivo tissues than cells cultured in 2D.[56] In cancer progression, a tumor mass can remodel its extracellular matrix so that fibril components are arranged radially to assist migration from its primary site.[57] As a demonstrative application in 3D cell culture, suspended fiber devices were used to guide cellular proliferation and migration in 3D from a dense cluster of glioblastoma cells. Glioblastoma multiforme is the most aggressive form of brain cancer. The suspended fiber experimental configuration is designed to offer topographic and mechanical biomimicry to white matter tracts, which is a common anatomical site where cancer propagates in brain tissue.[58,59] In the experiment, the fibrous components of suspended fiber devices do not require either surface treatment or other postprocessing to facilitate cell adhesion or stabilization of the microstructure. A chemical cross-linker was added to the solution prior to processing into fibers to make the structure insoluble to cell media. Given that the fibers are a gelatin hydrogel, the presence of linear Arg-Gly-Asp (RGD) sequences[60] provides sites of attachment for integrins, enabling cell adhesion and spreading.[61] Glioblastoma (U87) brain cancer cells are seeded directly from a cell aggregate onto a single suspended fiber layer, which permits migratory growth from the compacted aggregate and assembly into distinct 3D morphologies.

Figure 7 explores the way in which planar fiber patterns influence the macroscale cell aggregate morphology in 3D and how this relates to cell survival. Figure 7a–d depicts the morphology of suspended cell aggregates after 10 days of

DOI: 10.1021/acsami.9b01258
ACS Appl. Mater. Interfaces 2019, 11, 19679–19690

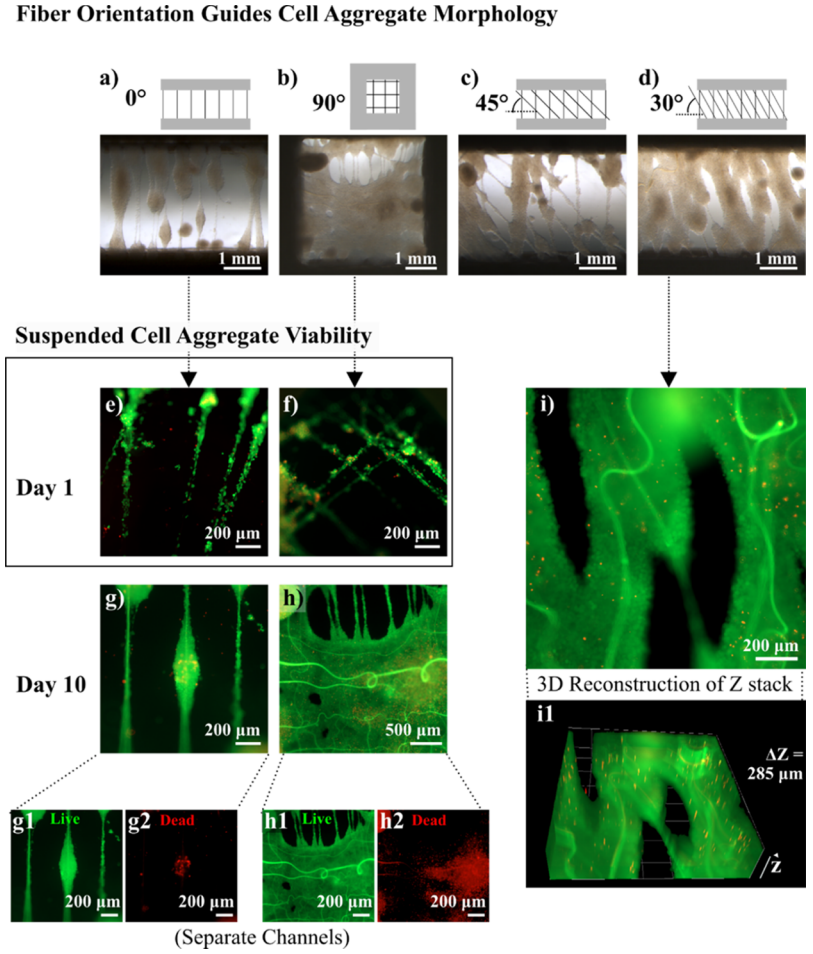

Figure 7. Suspended fiber patterns guide (U87) cell aggregate morphology. (a–d) Suspended fiber devices with different in-plane patterns provide topographic guidance for fusion and expansion of suspended cell aggregates over 10 days. A viability assay highlights the survival of cell aggregates cultured on suspended fiber devices at (e, f) day 1 and (g–i) day 10. (g1, g2, h1, h2) Separate live and dead intensities recorded from an aggregate-on-string and suspended cell sheet cultured over 10 days. (i1) 3D reconstruction of a *z*-stack acquired for a suspended aggregate grown on a suspended fiber device with fibers offset by 30° (i).

culture, guided by suspended fiber devices with different in-plane patterns. Figure 7a is designed with a single aligned fiber layer, whereas the samples in Figure 7b–d have a second fiber layer placed 100 μm above and offset by 90°, 45°, and 30°, respectively. The offset placement of fibers from one another, and junctions that patterning creates, improves the initial capture of cell aggregates on the fibers, and the topography guides the spread of cells from an aggregate, enhancing proliferation. The single-layer suspended fiber device, without an offset, produces an "aggregate-on-string" morphology, extending from the fiber axis and, in some cases, merging with neighbors. Interestingly, the cell aggregates cultured on suspended fiber devices with a patterned offset reflect the original orientation of the fibers before cell seeding, even following 10 days of culture, and the innate tendency of the fibers to undergo hydrogel swelling. The fiber patterns with an offset of 90° and 30° form an almost continuous cell "sheet". Figure 7e–i highlights the survival of aggregates cultured on suspended fibers without an offset and with a 90° offset at day 1 (Figure 7e,f) and day 10 (Figure 7g,h). At day 1, cell strings formed on both devices, and there is little to distinguish the viability of both. By day 10, the smaller aggregate in Figure 7g is almost completely viable, whereas the much larger fused aggregate sheet in Figure 7h was viable on the surface but had a necrotic core. This is consistent with common spheroid cultures, given that the diffusion limit of cells is around 100–200 μm[62] and there is no equivalent vasculature system in place. Figure 7g1,g2,h1,h2 displays the separate live and dead intensities recorded from an aggregate-on-string and suspended cell sheet. Figure 7i shows one slice of a 285 μm 2D *z*-stack image of a typical suspended aggregate cultured on fibers with a 30° offset. To convey the 3D nature of the aggregate, an animation of the *z*-stack accompanies Movie S1 (Supporting Information), and a computer-generated 3D reconstruction is presented in Figure 7i1.

Next, a comparatively lower density of cells was cultured on a suspended fiber device with a 90° offset to observe cell migration and fiber-guided dynamic aggregate formation. Figure 8a–e captures the process from day 1 to 13. Magnified panels in Figure 8a contrast A1, a cell-dense region, to A2, a region with a sparse cell population. After 2 days, there is visual evidence that cells have migrated from the concentrated region spreading far across the device. Magnified panels B1 and C1 show the same region of the device as A2 on day 3 (Figure 8b) and day 5 (Figure 8c), respectively. Panel C1 shows a small cell aggregate, indicating how the aggregation can fuse fibers together by carrying out nonaxial deformation on the fibers. The low apparent stiffness of the fibers is biomimetic of fibril

DOI: 10.1021/acsami.9b01258
ACS Appl. Mater. Interfaces 2019, 11, 19679–19690

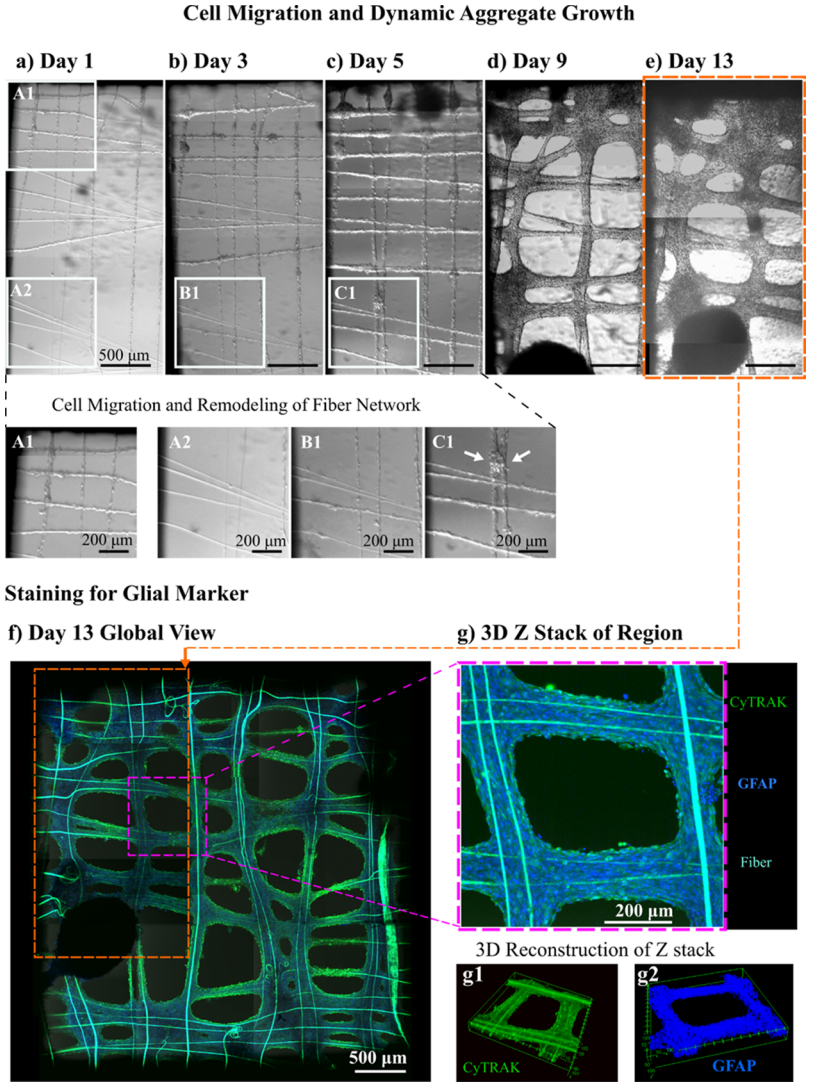

Figure 8. Cell migration and dynamic aggregate growth. Over 13 days (a–e), U87 cell aggregates migrate from a concentrated region (A1) on a suspended scaffold device, coating all the fibers within 5 days (A2, B1, C1). The white arrow in (C1) shows a magnified view of a cell aggregate at day 5 that has performed nonaxial deformation on a couple of fibers, fusing them together. (f) Global view of the aggregate morphology after 13 days; the cell nuclei are stained blue with CyTRAK and the GFAP in green stains for glial cytoskeletal markers. (g) Compiled projection of a *z*-stack of images taken at a smaller region; (g1, g2) 3D reconstruction of that *z*-stack at different angles for the separate staining channels.

components of the extracellular matrix, facilitating adequate cell–cell and cell–substrate interactions for the cell aggregates to remodel the fiber network. Figure 8f shows a global view of the suspended fiber device at day 13 after staining for nucleic and glial markers, confirming the astrocytic origin of the cells. An orange outline indicates the region of the device depicted in Figure 8a–e, and a pink outline marks a small region of interest analyzed as a *z*-stack in Figure 8g. Between days 1 and 13, cells have distributed themselves relatively uniformly on the suspended fiber device. Figure 8g shows a projection of a *z*-stack with a depth of 151.16 μm (Movie S2), and computer-generated 3D reconstructions of the *z*-stack in Figure 8g1,g2 show different angles of the structure in 3D with separate stained markers. Individual blue dots can only just be distinguished around the edges of the stained sample in Figure 8g2, indicating the high density of cells grown on the suspended fiber device.

Previous works on the precursor 2D configuration demonstrate the versatility of suspended fiber membranes in supporting multiple cell types.[23,24] Another interesting future application could be utilization of suspended fiber devices to orient the alignment of myocytes and other cell types with functionality that relies on an ordered cell arrangement. The enhanced patterning within a given suspended plane and in-built height presents new avenues for guiding tissue self-assembly[63,64] and studying the behavior of cell spheroids and aggregate fusion in different 3D morphologies.

2.7. Comparison to Existing Techniques. Three-dimensional printing with multiple materials and processes is envisaged to bring innovation in design, research, and product manufacturing.[7,8,65,66] Many printing techniques are available, ranging from inkjet to fused filament fabrication (FFF). The associated printing mechanism controls the size and shape of the "building block":[67] in the instance of inkjet printing, this takes the form of a picoliter drop, and for FFF, this is a filament in the hundreds of micrometer range.[67] Different printing mechanisms also have bounded capabilities in terms of the materials or "ink" they can process.[8,66] Figure S7 summarizes the main groups of printing mechanisms for creating 2.5D or 3D structures, mapping the printed feature

DOI: 10.1021/acsami.9b01258
ACS Appl. Mater. Interfaces 2019, 11, 19679–19690

resolution of each, alongside the compatible ink viscoelastic properties. If the attributes of solution electrospinning are incorporated, its capabilities lie in a region, which is not covered by existing printing mechanisms.[66] There is also the potential to adapt the multiprocess printing and fiber patterning strategy of 3D-LEP to other electrohydrodynamic writing approaches. To our knowledge, 3D-LEP offers unique competitive competences of creating microscale layered fibrous structures, over a centimeter in height, from a mild solution-based electrospinning process. Employing a solution-based approach has the benefit of compatibility with a wide choice of materials. This provides great versatility to design mesoscale fibers with material functionalities that can integrate with other functional components, printed by multiple fabrication techniques,[7,35] beyond what we demonstrate here with FFF printing. Additionally, solution-based electrospinning strategies offer a scope to innovate mild processing conditions. LEP demonstrates the scope to optimize solvent or polymer conditions, which allow subkilovolt processing at ambient temperature, compatible with patterning thermally or electrically sensitive elements,[24] including living organisms, as demonstrated with *Escherichia coli*.[23]

3. CONCLUSIONS

This study presented a novel method of fabricating suspended mesofiber structures by integrating low-voltage, solution electrospinning patterning with fused filament fabrication (FFF). 3D-LEP provides a unique capability of patterning suspended submicrometer to microscale fibers in 3D space, offering versatility in the vertical spacing of fiber layers, and patterning in-plane fiber orientation and density. The method offers potential compatibility for a broad range of fiber materials drawn from solution, including soft bioactive components. The low-voltage processing conditions are suited to applications with delicate material components, contained either in the patterned solution or within the substrate fibers are deposited on. The results were obtained on an open-source configuration with a tool switchover mechanism that is rapid and robust, which circumvents the typically time-consuming and tailored demands of microfabrication processes. The systematic characterization of the suspended behavior of the fibers with respect to a combination of applied voltages and support structure geometries led to a predictive fiber suspension guide to inform the design of new fibrous architectures. Applications in 3D cell culture were demonstrated, utilizing suspended fiber architectures as a versatile scaffolding device to facilitate guided self-assembly of cellular macrostructures. The ability to use computer-aided manufacturing to automate the assembly of fibrous architecture creates design avenues in coupling mesofiber chemistry and 3D architectures in a customizable fashion. By making the configuration open access and documenting our technical design process, we hope this work can serve as an exploratory guide to realize multimaterial cross-length scale prints with functional mesofiber architectures in three dimensions.

4. EXPERIMENTAL METHODS

4.1. Experimental Configuration. The 3D-LEP system modified an Ultimaker 2 (Ultimaker, Netherlands) 3D Printer, which provided the robotic *X-Y-Z* translation and the FFF printing. The tool-heads and tool docking stations for FFF printing and LEP processes were partially based on the STL models from https://www.youmagine.com/designs/dual-head-ultimaker2. However, to allow for precision deposition and tool-head exchange, we modified the design of the tool-heads incorporating a kinematic coupling design to improve the mounted tool stability (see Figure S1; STL files available in the University of Cambridge open-source platform (https://git.uis.cam.ac.uk/x/)). The electrospinning module consists of pneumatic pressure control for dispensing solutions provided by an OB1 MK3 system (Elveflow, France), blunt metallic syringe tips (25 gauge, TE725050PK), a 1 mL syringe barrel, a syringe adapter (401L-1, 900-250-6, Advanced Adhesive Solutions Ltd.), and a digital DC voltage source (Stanford Research, PS350). Experiments were performed under humidity of 60−80%.

4.2. Software Configuration. The firmware on the Ultimaker 2 3D printer was modified via Arduino IDE (Arduino) through the Marlin open-source repository on Github (https://github.com/Ultimaker/Ultimaker2Marlin). This allowed the printer to identify where to pick up and replace tool-heads for the FFF and LEP processes and permitted calibration of the coordinate system offsets. CAD models were designed and converted to STL files in Autodesk Inventor Professional 2017 (Autodesk Inc.). Simplify 3D slicer software was used to generate G-code. The electrospinning solution flow rate was modulated through the pressure supplied to the syringe barrel from an Elveflow microfluidic flow control system directed by the proprietary Elveflow ESI software (Elveflow, France).

4.3. Assessment of Tool-Head Stability. The electrospinning tool-head stability was assessed during a tool-changing sequence using images taken with a digital camera (Canon EOS 550D) with macro lens (Canon EF 100 mm Macro). The images were analyzed in Matlab using a color thresholder to measure the calibrated distance and any displacements during the tool changeover in micrometers between the tip of the syringe and a reference point in *X* and *Z*, as illustrated in Figure S2. The distance and displacements in *Y* were calculated by taking images at a shallow angle (25°) and using trigonometric functions to make a correction. The sequence of switching over the tool-heads while recording the image data was repeated 50 times in *X* and *Z* and 45 times in *Y* to collect a robust set of data.

4.4. LEP of Suspended Gelatin Mesofibers. A gelatin solution with a concentration of 19 wt % was prepared from porcine gelatin (porcine skin, Sigma-Aldrich) in a previously optimized solution of weight ratio of 33:22:26 acetic acid, ethyl acetate, and deionized water, respectively.[68,69] To create the fluorescent images in Figure 6, a fluorescent dye was added to the solution by dissolving fluorescein sodium salt (Sigma-Aldrich) into the deionized water beforehand at a concentration of 25 mg/mL and then preparing the solution as described above. The 3D printer alternated between printing thermoplastic support structures and drawing LEP patterned fibers. For the LEP process, pressures in the range of 30−200 mbar were used to attain the adequate flow rate for drawing fibers from the solution. This variation was to compensate for changes in ambient conditions, which influence the solution rheology. Fiber drawing speed was set between 75 and 150 mm/s, although 100 mm/s gave the most consistent results. Voltages in the range of 0−600 V were used to establish the "parametric space" and to construct fiber patterns of different configurations. For 3D fiber structure construction, a pitch size of 100 μm and the applied electric field within the range of 60−200 V/mm are utilized at each fiber layer.

4.5. Morphological Characterization. Images of fiber structures were taken using a combination of a Leica optical microscope (Leica DMLM + EC3 camera, Leica Microsystems), a GX Capture microscope camera (GT Vision Ltd.), and digital cameras (Motorola Play X smartphone and Canon EOS 700D DSLR with a Canon EF-S 18−135 mm macro lens and Kenko automatic extension tube set).

The fiber diameter measurements were taken from scanning electron microscopy (Helios NanoLab 650 DualBeam, FEI) images. Six samples of suspended fiber channel devices fabricated under control manufacturing conditions were analyzed. PLA scaffold parameters: H = 1.5 mm, L = 3 mm, P = 200 μm. Fiber spinning conditions: 150 V applied voltage and 125 mm/s translation speed. Between 23 and 33 individual fibers were imaged for each sample in ImageJ, taking an average of three measurements for each fiber.

DOI: 10.1021/acsami.9b01258
ACS Appl. Mater. Interfaces 2019, 11, 19679−19690

4.6. Mechanical Characterization. Young's modulus of the fibers was measured using an isometric force sensor (UF1 isometric force sensor, Applied Measurements Ltd.) mounted on a linear translation stage, coupled to a strain gauge, micro-stepper motor driver, and voltage supply. The resistive force sensed at the probe from the fibers and the probe displacement data was transferred using a USB serial converter (NI USB-6211, National Instruments) and recorded with a LabVIEW program (National Instruments). The data was analyzed in Origin (OriginLabs Corp., USA) software.

4.7. Biological Experiments. The gelatin solution was cross-linked with glyoxal at a concentration of 6% (v/v) prior to processing into fibers to prevent degradation in cell media. After suspended fiber device construction, the devices were sterilized under UV radiation for 20 min before soaking in cell culture medium 24 h before cell seeding. Human glioblastoma cells, U-87 (ATCC, HTB-14), were cultured in Dulbecco's modified Eagle's medium (DMEM, Invitrogen) supplemented with 10% fetal bovine serum (FBS, Sigma-Aldrich) under 5% CO_2 at 37 °C incubation. Cells were seeded as aggregates direct from a centrifuged cell pellet on suspended fiber devices designed with different fiber orientations: a single aligned layer and two aligned layers with offsets of 30°, 45°, and 90°. For the viability study, a seeding volume of 2 μL of cell pellet was used for each scaffold; samples were cultured for up to 10 days and imaged with optical microscopy. LIVE/DEAD viability/cytotoxicity assays (ThermoFisher Scientific L3224) were performed on the samples following manufacturer's protocol on days 1 and 10 and imaged with a Zeiss Axio Observer Z1 fluorescence microscope. For the migration and dynamic aggregate morphology study, a seeding volume of 1 μL of cell pellet was cultured on a suspended fiber device with a 90° offset for 13 days. Immunostaining with CyTRAK Orange (Fisher Scientific, 15540617) and Alexa Fluor 488 anti-GFAP (Life Technologies, 53-9892-82) was completed, and the sample was imaged with a Leica SP5 confocal microscope. Further details of the imaging methods and immunostaining are available in the Supporting Information.

■ ASSOCIATED CONTENT

Supporting Information

The Supporting Information is available free of charge on the ACS Publications website at DOI: 10.1021/acsami.9b01258.

Animation of a *z*-stack of fluorescent images of a suspended cell aggregate stained with LIVE/DEAD assay, as presented in Figure 7 (AVI)

Animation of a *z*-stack of fluorescent images of a fiber-guided cell aggregate stained with CyTRAK and GFAP, as presented in Figure 8 (AVI)

Details of the design of the 3D-LEP tool-head; design illustrations; assessment of the stability of tool-head exchange; images collected as part of the parametric characterization; SEM imaging of fiber merging; illustration of the mechanical testing; further demonstration of the patterning possible with 3D-LEP; a schematic capturing the state-of-the-art 3D printing in terms of printed resolution and ink viscoelastic properties; table with the supporting references, figures, and theory applied to infer details from the data presented; and additional experimental details of the staining and imaging procedures for the biological experiments (PDF)

■ AUTHOR INFORMATION

Corresponding Author

*E-mail: yysh2@cam.ac.uk.

ORCID

Yan Yan Shery Huang: 0000-0003-2619-730X

Author Contributions

E.L.G. and Y.Y.S.H. wrote the main manuscript text. E.L.G. performed the experiments and prepared the figures, unless otherwise stated. Y.Y.S.H. conceived and supervised the project. S.W. modified the firmware on the printer to facilitate picking up and printing with a secondary tool-head. M.G. provided the U87 cell line and performed the immunostaining and confocal microscopy. P.C. designed the 3D-LEP tool-head, performed the stability characterization, and prepared illustrations in Figures S1b,c and S2a,b and Table S1 in the Supporting Information. D.Z. assisted with fluorescence microscopy for the live and dead imaging. X.L. invented the method for LEP in 2D. All authors reviewed the manuscript.

Notes

The authors declare no competing financial interest.

■ ACKNOWLEDGMENTS

This work was supported by the Engineering and Physical Sciences Research Council (EPSRC, EP/M018989/1) and European Research Council (ERC-StG, 758865), and E.L.G. was a grateful recipient of a WD Armstrong Trust Studentship. M.G. is a recipient of a Cambridge Centre CRUK Multidisciplinary studentship, and D.Z. gratefully acknowledges support from the China Scholarship Council. We thank the technical assistance provided by the technical staff in the Department of Engineering, in particular, Len Howlett, and Jon Rickard at the electron microscopy suite in the Cavendish Laboratory. Additionally, we are grateful to Karim Ouaras, Lukas Vasadi, and Pooya Davoodi for their helpful discussions. We also thank YouImagine user "UltiArjan" for the conceptual tool-changing design our system had adapted and the open-source community of Github.

■ REFERENCES

(1) Dai, Y.; Liu, W.; Formo, E.; Sun, Y.; Xia, Y. Ceramic Nanofibers Fabricated by Electrospinning and Their Applications in Catalysis, Environmental Science, and Energy Technology. *Polym. Adv. Technol.* **2011**, *22*, 326−338.

(2) Mercante, L. A.; Scagion, V. P.; Migliorini, F. L.; Mattoso, L. H. C.; Correa, D. S. Electrospinning-Based (Bio)Sensors for Food and Agricultural Applications: A Review. *TrAC, Trends Anal. Chem.* **2017**, *91*, 91−103.

(3) Kitsara, M.; Agbulut, O.; Kontziampasis, D.; Chen, Y.; Menasché, P. Fibers for Hearts: A Critical Review on Electrospinning for Cardiac Tissue Engineering. *Acta Biomater.* **2017**, *48*, 20−40.

(4) Ding, B.; Wang, M.; Wang, X.; Yu, J.; Sun, G. Electrospun Nanomaterials for Ultrasensitive Sensors. *Mater. Today* **2010**, *13*, 16−27.

(5) Xue, J.; Xie, J.; Liu, W.; Xia, Y. Electrospun Nanofibers: New Concepts, Materials, and Applications. *Acc. Chem. Res.* **2017**, *50*, 1976−1987.

(6) Lu, X.; Wang, C.; Wei, Y. One-Dimensional Composite Nanomaterials: Synthesis by Electrospinning and Their Applications. *Small* **2009**, *5*, 2349−2370.

(7) MacDonald, E.; Wicker, R. Multiprocess 3D Printing for Increasing Component Functionality. *Science* **2016**, *353*, aaf2093.

(8) Truby, R. L.; Lewis, J. A. Printing Soft Matter in Three Dimensions. *Nature* **2016**, *540*, 371−378.

(9) Zhang, Y.; Zhang, F.; Yan, Z.; Ma, Q.; Li, X.; Huang, Y.; Rogers, J. A. Printing, Folding and Assembly Methods for Forming 3D Mesostructures in Advanced Materials. *Nat. Rev. Mater.* **2017**, *2*, 17019.

(10) Soliman, S.; Pagliari, S.; Rinaldi, A.; Forte, G.; Fiaccavento, R.; Pagliari, F.; Franzese, O.; Minieri, M.; Di Nardo, P.; Licoccia, S.; Traversa, E. Multiscale Three-Dimensional Scaffolds for Soft Tissue

DOI: 10.1021/acsami.9b01258
ACS Appl. Mater. Interfaces 2019, 11, 19679−19690

Engineering via Multimodal Electrospinning. *Acta Biomater.* **2010**, *6*, 1227−1237.
(11) Bhardwaj, N.; Kundu, S. C. Electrospinning: A Fascinating Fiber Fabrication Technique. *Biotechnol. Adv.* **2010**, *28*, 325−347.
(12) Greiner, A.; Wendorff, J. H. Electrospinning: A Fascinating Method for the Preparation of Ultrathin Fibers. *Angew. Chem., Int. Ed.* **2007**, *46*, 5670−5703.
(13) Luo, G.; Teh, K. S.; Liu, Y.; Zang, X.; Wen, Z.; Lin, L. Direct-Write, Self-Aligned Electrospinning on Paper for Controllable Fabrication of Three-Dimensional Structures. *ACS Appl. Mater. Interfaces* **2015**, *7*, 27765−27770.
(14) He, J.; Xu, F.; Cao, Y.; Liu, Y.; Li, D. Towards Microscale Electrohydrodynamic Three-Dimensional Printing. *J. Phys. D: Appl. Phys.* **2016**, *49*, No. 055504.
(15) He, J.; Xu, F.; Dong, R.; Guo, B.; Li, D. Electrohydrodynamic 3D Printing of Microscale Poly (ε -Caprolactone) Scaffolds with Multi-Walled Carbon Nanotubes. *Biofabrication* **2017**, *9*, No. 015007.
(16) Sun, D.; Chang, C.; Li, S.; Lin, L. Near-Field Electrospinning. *Nano Lett.* **2006**, *6*, 839−842.
(17) Chen, H.; Malheiro, A. de B. F. B.; van Blitterswijk, C.; Mota, C.; Wieringa, P. A.; Moroni, L. Direct Writing Electrospinning of Scaffolds with Multidimensional Fiber Architecture for Hierarchical Tissue Engineering. *ACS Appl. Mater. Interfaces* **2017**, *9*, 38187−38200.
(18) Hrynevich, A.; Elçi, B. Ş.; Haigh, J. N.; McMaster, R.; Youssef, A.; Blum, C.; Blunk, T.; Hochleitner, G.; Groll, J.; Dalton, P. D. Dimension-Based Design of Melt Electrowritten Scaffolds. *Small* **2018**, *14*, 1800232.
(19) Wunner, F. M.; Mieszczanek, P.; Bas, O.; Eggert, S.; Maartens, J.; Dalton, P. D.; De-Juan-Pardo, E. M.; Hutmacher, D. W. Printomics: The High-Throughput Analysis of Printing Parameters Applied to Melt Electrowriting. *Biofabrication* **2019**, *11*, No. 025004.
(20) Coppola, S.; Vespini, V.; Nasti, G.; Gennari, O.; Grilli, S.; Ventre, M.; Iannone, M.; Netti, P. A.; Ferraro, P. Tethered Pyro-Electrohydrodynamic Spinning for Patterning Well-Ordered Structures at Micro- and Nanoscale. *Chem. Mater.* **2014**, *26*, 3357−3360.
(21) Coppola, S.; Nasti, G.; Todino, M.; Olivieri, F.; Vespini, V.; Ferraro, P. Direct Writing of Microfluidic Footpaths by Pyro-EHD Printing. *ACS Appl. Mater. Interfaces* **2017**, *9*, 16488−16494.
(22) Harfenist, S. A.; Cambron, S. D.; Nelson, E. W.; Berry, S. M.; Isham, A. W.; Crain, M. M.; Walsh, K. M.; Keynton, R. S.; Cohn, R. W. Direct Drawing of Suspended Filamentary Micro- and Nanostructures from Liquid Polymers. *Nano Lett.* **2004**, *4*, 1931−1937.
(23) Li, X.; Li, Z.; Wang, L.; Ma, G.; Meng, F.; Pritchard, R. H.; Gill, E. L.; Liu, Y.; Huang, Y. Y. S. Low-Voltage Continuous Electrospinning Patterning. *ACS Appl. Mater. Interfaces* **2016**, 32120.
(24) Li, Z.; Tuffin, J.; Lei, I. M.; Ruggeri, F. S.; Lewis, N. S.; Gill, E. L.; Savin, T.; Huleihel, L.; Badylak, S. F.; Knowles, T.; Satchell, S.C.; Welsh, G. I.; Saleem, M. A.; Huang, Y. Y. S. Solution Fibre Spinning Technique for the Fabrication of Tuneable Decellularised Matrix-Laden Fibres and Fibrous Micromembranes. *Acta Biomater.* **2018**, *78*, 111−122.
(25) Russo, P.; Nasti, G.; Coppola, S.; Gentile, G.; Tuccitto, N.; Li-Destri, G.; Marletta, G.; Ferraro, P. Single Fibres of Pyro-Electrospinned PVDF-HFP/MWCNT Unveal High Electrical Conductivity. *Polymer* **2018**, *159*, 157−161.
(26) Sun, B.; Long, Y. Z.; Zhang, H. D.; Li, M. M.; Duvail, J. L.; Jiang, X. Y.; Yin, H. L. Advances in Three-Dimensional Nanofibrous Macrostructures via Electrospinning. *Prog. Polym. Sci.* **2014**, *39*, 862−890.
(27) Wang, J.; Nain, A. S. Suspended Micro/Nanofiber Hierarchical Biological Scaffolds Fabricated Using Non-Electrospinning STEP Technique. *Langmuir* **2014**, *30*, 13641−13649.
(28) Li, D.; Wang, Y.; Xia, Y. Electrospinning of Polymeric and Ceramic Nanofibers as Uniaxially Aligned Arrays. *Nano Lett.* **2003**, *3*, 1167−1171.
(29) Kriebel, A.; Rumman, M.; Scheld, M.; Hodde, D.; Brook, G.; Mey, J. Three-Dimensional Configuration of Orientated Fibers as Guidance Structures for Cell Migration and Axonal Growth. *J. Biomed. Mater. Res., Part B* **2014**, *102*, 356−365.
(30) Wunner, F. M.; Wille, M.-L.; Noonan, T. G.; Bas, O.; Dalton, P. D.; De-Juan-Pardo, E. M.; Hutmacher, D. W. Melt Electrospinning Writing of Highly Ordered Large Volume Scaffold Architectures. *Adv. Mater.* **2018**, *30*, 1706570.
(31) Kim, H. Y.; Lee, M.; Park, K. J.; Kim, S.; Mahadevan, L. Nanopottery: Coiling of Electrospun Polymer Nanofibers. *Nano Lett.* **2010**, *10*, 2138−2140.
(32) Chen, T.; Bakhshi, H.; Liu, L.; Ji, J.; Agarwal, S. Combining 3D Printing with Electrospinning for Rapid Response and Enhanced Designability of Hydrogel Actuators. *Adv. Funct. Mater.* **2018**, *28*, 1800514.
(33) Park, S. H.; Kim, T. G.; Kim, H. C.; Yang, D.-Y.; Park, T. G. Development of Dual Scale Scaffolds via Direct Polymer Melt Deposition and Electrospinning for Applications in Tissue Regeneration. *Acta Biomater.* **2008**, *4*, 1198−1207.
(34) de Ruijter, M.; Hrynevich, A.; Haigh, J. N.; Hochleitner, G.; Castilho, M.; Groll, J.; Malda, J.; Dalton, P. D. Out-of-Plane 3D-Printed Microfibers Improve the Shear Properties of Hydrogel Composites. *Small* **2018**, *14*, 1702773.
(35) de Ruijter, M.; Ribeiro, A.; Dokter, I.; Castilho, M.; Malda, J. Simultaneous Micropatterning of Fibrous Meshes and Bioinks for the Fabrication of Living Tissue Constructs. *Adv. Healthcare Mater.* **2018**, 1800418.
(36) Fattahi, P.; Dover, J. T.; Brown, J. L. 3D Near-Field Electrospinning of Biomaterial Microfibers with Potential for Blended Microfiber-Cell-Loaded Gel Composite Structures. *Adv. Healthcare Mater.* **2017**, *6*, 1700456.
(37) Brown, T. D.; Edin, F.; Detta, N.; Skelton, A. D.; Hutmacher, D. W.; Dalton, P. D. Melt Electrospinning of Poly(ε-Caprolactone) Scaffolds: Phenomenological Observations Associated with Collection and Direct Writing. *Mater. Sci. Eng. C* **2014**, *45*, 698−708.
(38) Sampson, S. L.; Saraiva, L.; Gustafsson, K.; Jayasinghe, S. N.; Robertson, B. D. Cell Electrospinning: An in Vitro and in Vivo Study. *Small* **2014**, *10*, 78−82.
(39) Townsend-Nicholson, A.; Jayasinghe, S. N. Cell Electrospinning: A Unique Biotechnique for Encapsulating Living Organisms for Generating Active Biological Microthreads/Scaffolds. *Biomacromolecules* **2006**, *7*, 3364−3369.
(40) He, J.; Zhao, X.; Chang, J.; Li, D. Microscale Electro-Hydrodynamic Cell Printing with High Viability. *Small* **2017**, *13*, 1702626.
(41) Nagarajan, S.; Soussan, L.; Bechelany, M.; Teyssier, C.; Cavaillès, V.; Pochat-Bohatier, C.; Miele, P.; Kalkura, N.; Janot, J.-M.; Balme, S. Novel Biocompatible Electrospun Gelatin Fiber Mats with Antibiotic Drug Delivery Properties. *J. Mater. Chem. B* **2016**, *4*, 1134−1141.
(42) Ghosh, S. K.; Adhikary, P.; Jana, S.; Biswas, A.; Sencadas, V.; Gupta, S. D.; Tudu, B.; Mandal, D. Electrospun Gelatin Nanofiber Based Self-Powered Bio-e-Skin for Health Care Monitoring. *Nano Energy* **2017**, *36*, 166−175.
(43) Kharaziha, M.; Nikkhah, M.; Shin, S.-R.; Annabi, N.; Masoumi, N.; Gaharwar, A. K.; Camci-Unal, G.; Khademhosseini, A. PGS:Gelatin Nanofibrous Scaffolds with Tunable Mechanical and Structural Properties for Engineering Cardiac Tissues. *Biomaterials* **2013**, *34*, 6355−6366.
(44) Slocum, A. H. Design of Three-Groove Kinematic Couplings. *Precis. Eng.* **1992**, *14*, 67−76.
(45) Tian, F.; Hosseinkhani, H.; Hosseinkhani, M.; Khademhosseini, A.; Yokoyama, Y.; Estrada, G. G.; Kobayashi, H. Quantitative Analysis of Cell Adhesion on Aligned Micro- and Nanofibers. *J. Biomed. Mater. Res., Part A* **2008**, *84A*, 291−299.
(46) Theron, S. A.; Zussman, E.; Yarin, A. L. Experimental Investigation of the Governing Parameters in the Electrospinning of Polymer Solutions. *Polymer* **2004**, *45*, 2017−2030.
(47) Reneker, D. H.; Yarin, A. L. Electrospinning Jets and Polymer Nanofibers. *Polymer* **2008**, 2387−2425.

DOI: 10.1021/acsami.9b01258
ACS Appl. Mater. Interfaces 2019, 11, 19679−19690

(48) Huang, Y. Y. S.; Terentjev, E. M.; Oppenheim, T.; Lacour, S. P.; Welland, M. E. Fabrication and Electromechanical Characterization of Near-Field Electrospun Composite Fibers. *Nanotechnology* **2012**, *23*, 105305.
(49) Bellan, L. M.; Kameoka, J.; Craighead, H. G. Measurement of the Young's Moduli of Individual Polyethylene Oxide and Glass Nanofibres. *Nanotechnology* **2005**, *16*, 1095−1099.
(50) Timoshenko, S. *Strength of Materials*; 3 rd ed.; Van Nostrand: Princeton, NJ :, 1940.
(51) Huang, Z.-M.; Zhang, Y. Z.; Ramakrishna, S.; Lim, C. T. Electrospinning and Mechanical Characterization of Gelatin Nanofibers. *Polymer* **2004**, *45*, 5361−5368.
(52) Butcher, A. L.; Koh, C. T.; Oyen, M. L. Systematic Mechanical Evaluation of Electrospun Gelatin Meshes. *J. Mech. Behav. Biomed. Mater.* **2017**, *69*, 412−419.
(53) Tonsomboon, K.; Oyen, M. L. Composite Electrospun Gelatin Fiber-Alginate Gel Scaffolds for Mechanically Robust Tissue Engineered Cornea. *J. Mech. Behav. Biomed. Mater.* **2013**, *21*, 185−194.
(54) Middleton, R.; Li, X.; Shepherd, J.; Li, Z.; Wang, W.; Best, S. M.; Cameron, R. E.; Huang, Y. Y. S. Near-Field Electrospinning Patterning Polycaprolactone and Polycaprolactone/Collagen Interconnected Fiber Membrane. *Macromol. Mater. Eng.* **2018**, *303*, 1700463.
(55) Tonsomboon, K.; Butcher, A. L.; Oyen, M. L. Strong and Tough Nanofibrous Hydrogel Composites Based on Biomimetic Principles. *Mater. Sci. Eng. C* **2017**, *72*, 220−227.
(56) Pampaloni, F.; Reynaud, E. G.; Stelzer, E. H. K. The Third Dimension Bridges the Gap between Cell Culture and Live Tissue. *Nat. Rev. Mol. Cell Biol.* **2007**, *8*, 839−845.
(57) Frantz, C.; Stewart, K. M.; Weaver, V. M. The Extracellular Matrix at a Glance. *J. Cell Sci.* **2010**, *123*, 4195−4200.
(58) Rao, S. S.; Nelson, M. T.; Xue, R.; DeJesus, J. K.; Viapiano, M. S.; Lannutti, J. J.; Sarkar, A.; Winter, J. O. Mimicking White Matter Tract Topography Using Core−shell Electrospun Nanofibers to Examine Migration of Malignant Brain Tumors. *Biomaterials* **2013**, *34*, 5181−5190.
(59) Espinosa-Hoyos, D.; Jagielska, A.; Homan, K. A.; Du, H.; Busbee, T.; Anderson, D. G.; Fang, N. X.; Lewis, J. A.; Van Vliet, K. J. Engineered 3D-Printed Artificial Axons. *Sci. Rep.* **2018**, *8*, 478.
(60) Davidenko, N.; Schuster, C. F.; Bax, D. V.; Farndale, R. W.; Hamaia, S.; Best, S. M.; Cameron, R. E. Evaluation of Cell Binding to Collagen and Gelatin: A Study of the Effect of 2D and 3D Architecture and Surface Chemistry. *J. Mater. Sci.: Mater. Med.* **2016**, *27*, 148.
(61) Xing, Q.; Yates, K.; Vogt, C.; Qian, Z.; Frost, M. C.; Zhao, F. Increasing Mechanical Strength of Gelatin Hydrogels by Divalent Metal Ion Removal. *Sci. Rep.* **2015**, *4*, 4706.
(62) Lovett, M.; Lee, K.; Edwards, A.; Kaplan, D. L. Vascularization Strategies for Tissue Engineering. *Tissue Eng., Part B* **2009**, *15*, 353−370.
(63) Lancaster, M. A.; Corsini, N. S.; Wolfinger, S.; Gustafson, E. H.; Phillips, A. W.; Burkard, T. R.; Otani, T.; Livesey, F. J.; Knoblich, J. A. Guided Self-Organization and Cortical Plate Formation in Human Brain Organoids. *Nat. Biotechnol.* **2017**, *35*, 659−666.
(64) Tocchio, A.; Durmus, N. G.; Sridhar, K.; Mani, V.; Coskun, B.; El Assal, R.; Demirci, U. Magnetically Guided Self-Assembly and Coding of 3D Living Architectures. *Adv. Mater.* **2018**, *30*, 1705034.
(65) Gross, B. C.; Erkal, J. L.; Lockwood, S. Y.; Chen, C.; Spence, D. M. Evaluation of 3D Printing and Its Potential Impact on Biotechnology and the Chemical Sciences. *Anal. Chem.* **2014**, *86*, 3240−3253.
(66) Gill, E. L.; Li, X.; Birch, M. A.; Huang, Y. Y. S. Multi-Length Scale Bioprinting towards Simulating Microenvironmental Cues. *Bio-Design Manuf.* **2018**, *1*, 77−88.
(67) Hinton, T. J.; Lee, A.; Feinberg, A. W. 3D Bioprinting from the Micrometer to Millimeter Length Scales: Size Does Matter. *Curr. Opin. Biomed. Eng.* **2017**, 31.
(68) Song, J. H.; Kim, H. E.; Kim, H. W. Production of Electrospun Gelatin Nanofiber by Water-Based Co-Solvent Approach. *J. Mater. Sci. Mater. Med.* **2008**, *19*, 95−102.
(69) Xue, N.; Li, X.; Bertulli, C.; Li, Z.; Patharagulpong, A.; Sadok, A.; Huang, Y. Y. S. Rapid Patterning of 1-D Collagenous Topography as an ECM Protein Fibril Platform for Image Cytometry. *PLoS One* **2014**, *9*, No. e93590.

DOI: 10.1021/acsami.9b01258
ACS Appl. Mater. Interfaces 2019, 11, 19679−19690